Hindawi Publishing Corporation
The Scientific World Journal
Volume 2014, Article ID 508163, 12 pages
http://dx.doi.org/10.1155/2014/508163

Research Article

A Real-Time and Closed-Loop Control Algorithm for Cascaded Multilevel Inverter Based on Artificial Neural Network

Libing Wang,[1] Chengxiong Mao,[1] Dan Wang,[2] Jiming Lu,[2] Junfeng Zhang,[3] and Xun Chen[3]

[1] *State Key Laboratory of Advanced Electromagnetic Engineering and Technology, Huazhong University of Science and Technology, Wuhan 430074, China*
[2] *School of Electrical & Electronic Engineering, Huazhong University of Science and Technology, Wuhan 430074, China*
[3] *Electric Power Research Institute of Guangdong Power Grid Corporation, Guangzhou, Guangdong 510080, China*

Correspondence should be addressed to Dan Wang; wangdan@mail.hust.edu.cn

Received 8 October 2013; Accepted 19 January 2014; Published 16 March 2014

Academic Editors: E. M. Berkouk and M. Chomat

In order to control the cascaded H-bridges (CHB) converter with staircase modulation strategy in a real-time manner, a real-time and closed-loop control algorithm based on artificial neural network (ANN) for three-phase CHB converter is proposed in this paper. It costs little computation time and memory. It has two steps. In the first step, hierarchical particle swarm optimizer with time-varying acceleration coefficient (HPSO-TVAC) algorithm is employed to minimize the total harmonic distortion (THD) and generate the optimal switching angles offline. In the second step, part of optimal switching angles are used to train an ANN and the well-designed ANN can generate optimal switching angles in a real-time manner. Compared with previous real-time algorithm, the proposed algorithm is suitable for a wider range of modulation index and results in a smaller THD and a lower calculation time. Furthermore, the well-designed ANN is embedded into a closed-loop control algorithm for CHB converter with variable direct voltage (DC) sources. Simulation results demonstrate that the proposed closed-loop control algorithm is able to quickly stabilize load voltage and minimize the line current's THD (<5%) when subjecting the DC sources disturbance or load disturbance. In real design stage, a switching angle pulse generation scheme is proposed and experiment results verify its correctness.

1. Introduction

Multilevel converters have drawn tremendous research interest in recent years and have been implemented in several high-voltage and high-power applications. One of the multilevel topologies is cascaded H-bridges (CHB) configuration which needs several separated DC sources [1].

Various modulation strategies have been developed for CHB converter. Phase shifted PWM (PSPWM) and space vector PWM (SVPWM) are very popular methods in industrial applications [2]. Another important modulation method for CHB converter is the optimal PWM, which includes selective harmonic elimination PWM (SHE-PWM) and harmonic minimization strategies [3]. The main challenge associated with SHE-PWM technique is that a specified number of nonlinear equations must be solved to obtain the appropriate switching angles. Several analytical algorithms have been reported to solve these transcendental equations, such as iterative methods [4], theory of symmetric polynomials [5], and search optimization [6].

The harmonic pollution minimization in multilevel converter with staircase modulation strategy is often defined as a time-limited optimization problem in real-time applications. Modern evolution algorithms have also been used to determine the optimal switching pulses such as genetic algorithms (GA), particle swarm optimization (PSO) [7–9], shuffled-frog-leaping algorithm (SFLA), and Bee algorithm (BA) [10, 11]. In [12], a generalized formulation for multilevel SHE-PWM converters for any number of levels and any number of switching angles with both equal and unequal DC voltage levels was reported. The limitation of quarter-wave symmetrical waveform was relaxed, and half-wave [13] and nonsymmetrical waveforms [14] have also been reported. These papers assumed that the DC source levels do not vary with time. However, the DC voltage levels may vary with time in practice, and calculations methods

based on this assumption are very time-consuming. They can only be done by a computer offline. The offline calculated optimal switching angles have to be stored in a look-up table. For every solution in each possible DC voltage level case, a considerable large look-up table would be required. Therefore, the above methods cannot be implemented in real-time manner due to the overhead of computations.

In [15, 16], the authors developed a real-time algorithm to calculate the optimal switching angles. Although the resulted voltage THD is minimized, this iterative algorithm was complex. An alternate approach in which artificial neural network (ANN) is implemented was proposed to replace the look-up table and generate optimal switching angles [17]. However, this method still requires large memory to store numerous solutions and only open-loop control of CHB converter was considered.

In order to real-time-control the CHB converter with variable DC sources under staircase modulation strategy, a real-time and closed-loop control algorithm based on ANN for three-phase CHB converter is proposed in this paper. It needs little computation time and memory and has a good control capability of CHB converter. It has two steps. In the first step, HPSO-TVAC algorithm is employed to calculate the optimal switching angles offline. In second step, only 40 samples of optimal switching angles are used to train an ANN and design an ANN to generate optimal switching angles in a real-time manner. The designed ANN is easily embedded into the proposed closed-loop control algorithm. Simulation results demonstrate that the proposed closed-loop control algorithm can quickly stabilize load voltage and minimize the line current's THD (<5%) subjecting to DC sources disturbance and load disturbance.

The rest of the paper is arranged as follows. In Section 2, harmonic distortion minimization problem of CHB converter is described. In Section 3, the principle of HPSO-TVAC is introduced and compared with other traditional evolution optimization algorithms. In Section 4, ANN is introduced and designed. The proposed ANN is also compared with previous real-time optimization method. In Section 5, a closed-loop control algorithm for CHB converter is proposed, and the simulation results are given to demonstrate the performance of the proposed method in the presence of DC sources disturbance and load disturbance. In addition, the switching angle pulse generation issue is considered in real design stage. Finally, Section 6 concludes the paper.

2. Harmonic Minimization Problem

Figure 1(a) shows the structure of a three-phase CHB converter. Each unit has its own separated DC source with a variable voltage level. Figure 1(b) also shows that the ac terminal output phase voltage is synthesized by the sum of H-bridge voltages; that is, $v_{an} = v_{dc1} + v_{dc2} + \cdots + v_{dcs}$. Each full bridge can generate three different voltage levels: v_{dc}, 0, and $-v_{dc}$. The number of the levels m of output phase voltage in this topology is $m = 2s+1$, where s is the number of the DC sources. In the half-cycle waveform, the switching angles set $(\theta_1, \theta_2, \ldots, \theta_s)$ is symmetrically arranged. The next half-cycle waveform is similar, but with a negative sign.

The Fourier series expansions of the generated output phase voltage v_{an} are

$$v_{an} = \sum_{n=1}^{\infty} \left(a_n \sin n\alpha_n + b_n \cos n\alpha_n\right). \tag{1}$$

Owing to the quarter-wave symmetry of phase voltage, only odd harmonics are presented in v_{an} ($b_n = 0$). The amplitude of the nth harmonic a_n is expressed only with the first quadrant switching angles $\theta_1, \theta_2, \ldots, \theta_s$

$$a_n = \frac{4V_{dc}}{n\pi} \sum_{k=1}^{s} \cos\left(n\theta_k\right), \qquad 0 < \theta_1 < \theta_2 < \cdots < \theta_s < \frac{\pi}{2}, \tag{2}$$

where s is the number of variables corresponding to switching angles $\theta_1 \sim \theta_s$ of the first quadrant; V_{dc} is the rated DC voltage level.

In the traditional SHE-PWM method, a_n was assigned as the desired value for fundamental component and equated to zero for the harmonics to be eliminated. Nonlinear transcendental equations were formulated and solved by analytical algorithms. As mentioned, reliability of the results of these nonlinear equations severely depends on the initial guess, and solutions were not available at some points.

In order to avoid these problems, another method is applied to convert the SHE-PWM problem into an optimization problem. In this method, the objective function is to minimize a quality factor such as total harmonic distortion (THD) or distortion harmonic index (DHI). In this study, THD up to the 49th harmonics order is considered as the objective function. The voltage THD is formulated as

$$\text{THD\%} = \frac{\sqrt{\sum_{n=5,7,\ldots}^{49} a_n^2}}{a_1} \times 100. \tag{3}$$

The voltage THD is considered as the objective function $F(\theta)$ in the evolution algorithm. Hence, the minimization problem and its constraints can be represented in a mathematical form as follows:

$$\begin{aligned} &\text{Min } F(\theta) = \text{THD\%} \\ &\text{Sub.: } 0 < \theta_1 < \theta_2 < \cdots < \theta_m < \frac{\pi}{2}; \\ &a_1 = M; \\ &a_5 \le \varepsilon_5; \\ &a_7 \le \varepsilon_7; \\ &a_i \le \varepsilon_i, \end{aligned} \tag{4}$$

where M is the amplitude of the desired fundamental component, $\varepsilon_5, \varepsilon_7, \ldots, \varepsilon_{49}$ are the allowable limits of individual harmonics mandatory required by Grid Standards [18]. The triple harmonics do not exist in three-phase power system. In this study, a novel PSO is employed to optimize the objective function as described in Section 3.

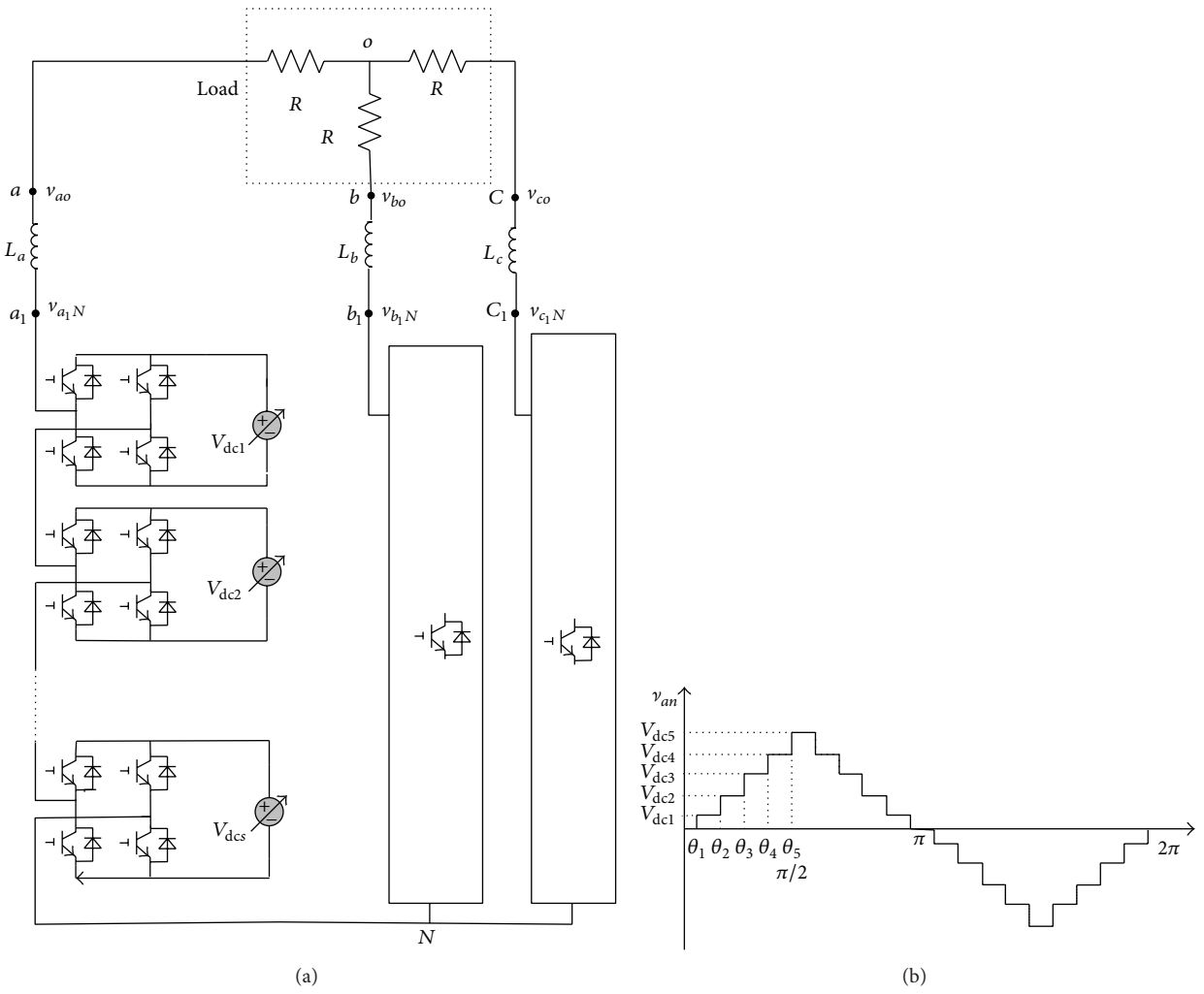

FIGURE 1: (a) The structure of a three-phase CHB inverter and (b) output phase voltage v_{an} of inverter based on the staircase modulation strategy.

3. Self-Organizing Hierarchical Particle Swarm Optimizer with Time-Varying Acceleration Coefficients

In this section, self-organizing hierarchical particle swarm optimizer with time-varying acceleration coefficient (HPSO-TVAC) is introduced [19] and applied to solve the above harmonic minimization problem. In addition, a comparison with traditional evolution optimizers, such as GA, SFLA, and BA, indicates that HPSO-TVAC gives the best solutions in a wide range of modulation index.

3.1. Basic PSO. The basic PSO initiates a random initialization of a population of particles in the search space. Each particle is a potential solution for the optimization problem and tries to search the best position in the total search space. The social behavior of particles that was modeled in the PSO algorithm is used to find the global best solution by simply adjusting each particle's velocity according to its own flying experience and adjusting each particle's position according to the other particles' flying experience.

Each particle is described in the d-dimensional search space by the position vector $X_i = [x_{i1}, x_{i2}, \ldots, x_{id}]$ and the velocity vector $V_i = [v_{i1}, v_{i2}, \ldots, v_{id}]$. In the swarm, the best position of each particle found so far (refer to the optimum fitness function value of each particles) is defined as local best position and is denoted by $P_i = [p_{i1}, p_{i2}, \ldots, p_{id}]$, and the global best position of the swarm found so far (refer to the optimum fitness function value of all particles) is denoted by $P_g = [p_{g1}, p_{g2}, \ldots, p_{gd}]$. Then, the new velocity of the ith particle on the jth dimension is updated by using (5) and the position of each particle is updated by using (6):

$$v_{ij}(t+1) = w\left[v_{ij}(t) + \varphi_1 r_1\left(p_{ij} - x_{ij}(t)\right) + \varphi_2 r_2\left(p_{gj} - x_{ij}(t)\right)\right], \quad (5)$$

$$x_{ij}(t+1) = x_{ij}(t) + v_{ij}(t+1), \quad (6)$$

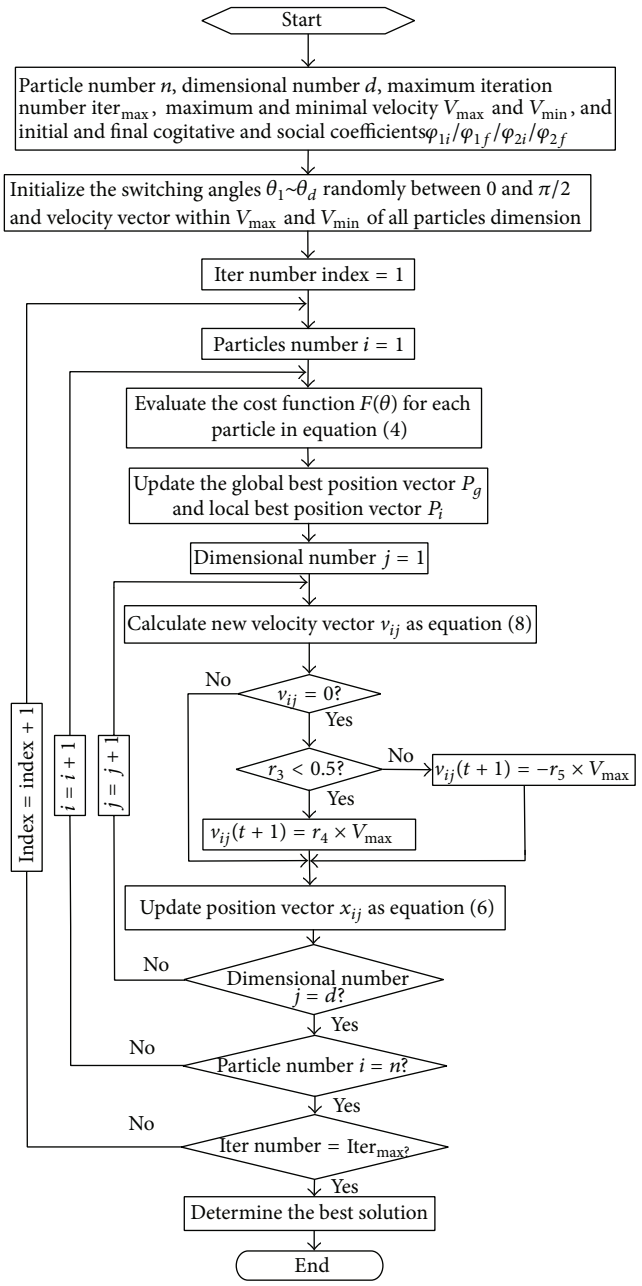

Figure 2: Flow chart of HPSO-TVAC applying to harmonic minimization problem.

where φ_1 and φ_2 are constants known as cogitative and social coefficients, respectively; r_1 and r_2 are random values uniformly distributed within $[0, 1]$. $v_{ij}(t)$ is the previous velocity term. The constriction factor ω is used to promise the convergence of the algorithm and defined as

$$w = \frac{2}{\left|2 - \varphi - \sqrt{\varphi^2 - 4\varphi}\right|} \quad (\varphi = \varphi_1 + \varphi_2,\ \varphi > 4). \tag{7}$$

Typically, φ is set to 4.1, and the constriction factor ω is set to 0.729 [20].

3.2. Harmonic Minimization Using HPSO-TVAC. Even though the basic PSO is capable of locating a good solution at a fast rate, its ability to fine tune the global optimum solution is comparatively weak, which is mainly due to lack of diversity at the end of search progress. Thus, HPSO-TVAC is used to solve this problem.

In this novel PSO strategy, the previous velocity term $v_{ij}(t)$ in (5) is made zero, and particles rapidly rush towards a local optimum point because of lack of momentum. When a particle stagnates, its local best position P_i remains unchanged for a number of iterations. When all particles stagnate, the algorithm converges prematurely to a local optimal point and global position P_g remains unchanged and v_{ij} becomes zero. In order to provide the required momentum for particles to find the global optimum solution in this case, the velocity vector of a particle is reinitialized with a random velocity. In this algorithm, the new velocity of the ith particle on the jth dimension is updated as follows:

$$v_{ij}(t+1) = \begin{bmatrix} \left(\left(\varphi_{1f} - \varphi_{1i}\right)\dfrac{\text{iter}}{\text{iter}_{\max}} + \varphi_{1i}\right) r_1 \left(p_{ij} - x_{ij}(t)\right) \\ + \left(\left(\varphi_{2f} - \varphi_{2i}\right)\dfrac{\text{iter}}{\text{iter}_{\max}} + \varphi_{2i}\right) r_2 \left(p_{gj} - x_{ij}(t)\right) \end{bmatrix}, \tag{8}$$

$$\begin{aligned} &\text{if } v_{ij} = 0 \text{ and } r_3 < 0.5 \\ &v_{ij}(t+1) = r_4 \times V_{\max}; \\ &\text{else} \\ &v_{ij}(t+1) = -r_5 \times V_{\max}; \\ &\text{end.} \end{aligned} \tag{9}$$

φ_{1i} and φ_{1f} are initial and final cogitative coefficients; φ_{2i} and φ_{2f} are initial and final social coefficients; iter and $\text{iter}_{\max}$ are current number of iterations and maximum number of iteration; $r_1 \sim r_5$ are randomly numbers between $[0, 1]$; $V_{\max}$ is the maximum velocity value.

Thus, a series of particle swarm optimizers are generated inside the main PSO algorithm until the convergence criteria are reached. More details about the HPSO-TVAC were presented in [19]. Appling HPSO-TVAC to the harmonic minimization problem described in above section, the procedure is presented in Figure 2, and the results of optimal switching angles are presented in Figure 3.

3.3. Comparison of Traditional Evolution Optimizer. In order to illustrate the efficiency of the applied approach, a comparison between other three evolution optimizers including GA, SFLA, and BA is performed at five operating points of CHB converter. The parameters of these traditional evolution optimizers are set the same as HPSO-TVAC for fair comparison. The operating point is described by the desired modulation

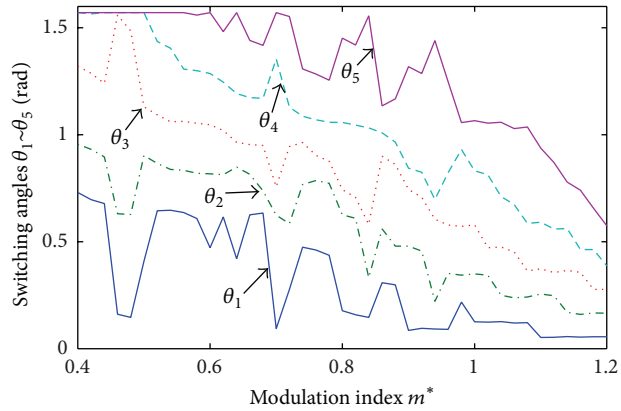

Figure 3: Calculated switching angles $\theta_1 \sim \theta_5$ by HPSO-TVAC.

Table 1: Parameters of evolution optimizers.

Parameters	HPSO-TVAC	GA	SFLA	BA
Population size	100	100	100	100
Iteration number	500	500	500	500
Number of runs	10	10	10	10
$\varphi_{1i}/\varphi_{1f}/\varphi_{2i}/\varphi_{2f}$	2.5/0.2/0.2/2.2			
$\varepsilon_5/\varepsilon_7 \cdots/\varepsilon_{49}/\%$	$5/4/3/\cdots/0.2 + 25/h$			
Modulation index rang	0.4–1.2			
Calculation step of m^*	0.01			

Table 2: Calculated switching angles by different methods at operating point ($m^* = 1.0$).

Method	θ_1/rad	θ_2/rad	θ_3/rad	θ_4/rad	θ_5/rad	THD%
HPSO	0.1256	0.3495	0.5788	0.8310	1.0655	4.17
GA	0.1269	0.3455	0.5738	0.8192	1.0799	4.32
SFLA	0.1352	0.3476	0.5731	0.8336	1.0648	4.26
BA	0.1238	0.3480	0.8345	0.5785	1.0636	4.18

index m^* which is defined as normalized value of the desired fundamental component. m^* is given as follows:

$$m^* = \frac{M}{sV_{dc}}. \tag{10}$$

Table 1 shows the parameters of HPSO-TVAC and other three evolution optimizers. The number of switching angles is set to five ($s = 5$) and five equal DC sources ($V_{dc} = 20$ V) are considered in the case. The inequality constraint limits ($\varepsilon_5, \varepsilon_7, \ldots, \varepsilon_{49}$) in (4) are also shown in Table 1. Table 2 depicts the calculated switching angles $\theta_1 \sim \theta_5$ and the resulting THD by each method. THD is computed for harmonics up to 49 orders. Table 3 shows the resulting THD and the variance of THD by each method running 10 times at five operating points ($m^* = 0.4, 0.5, 0.8, 1.0, 1.1$).

According to Tables 2 and 3, HPSO-TVAC method produces the smallest THD and the smallest variance of THD in 10 times running. This means that HPSO-TVAC can provide the most stable solution in a wide range of modulation index. In real-time design application, a stable algorithm is important to avoid losing solutions in some operating points and to produce a continuous solution trajectory. The applied approach is more stable and more effective than GA, SFLA, and BA optimizer in harmonic pollution minimization problem.

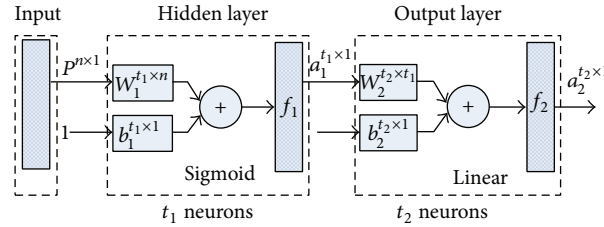

Figure 4: Structure of two-layer feed-forward network.

Table 3: THD results and variance of THD in 10 times running at five operating points.

m^* THD%/variance	GA	BA	SFLA	HPSO-TVAC
0.4	12.28/0.03	12.15/0.06	12.11/0.02	12.10/0.02
0.6	6.61/0.03	5.89/0.06	6.70/0.02	5.78/0.01
0.8	5.39/0.04	4.93/0.05	4.83/0.01	4.82/0.01
1.0	4.32/0.04	4.18/0.07	4.26/0.03	4.17/0.02
1.1	4.22/0.04	4.19/0.07	4.22/0.02	4.09/0.01

4. Artificial Neural Networks

ANN is a powerful tool to control a nonlinear system that is very complex in nature. A well-designed ANN can be used to replace the look up table and to generate optimal switching angles in a real-time manner [21].

4.1. Structure of ANN. ANN consists of a number of fundamental elements named neurons that are organized in several layers. Every neuron has an input vector P with s inputs. The neuron multiples input vector P by a weight matrix W and is summed with a bias vector b. Then a transfer function f is applied on the above results, which produces the output vector of the neuron $f(WP + b)$ [22, 23].

A typical two-layer feed-forward network shown in Figure 4 with sigmoid hidden neurons and linear output neurons can fit multidimensional mapping problems arbitrarily well. There are n inputs and vectors P in an input layer, t_1 sigmoid hidden neurons in hidden layer, and t_2 linear output neurons in output layer. The weight matrix W_i of ith layer with t_i neurons is a $t_i \times t_{i-1}$ matrix. The bias vector b_i of ith layer is a $t_i \times 1$ one and the produced output vector is a $t_i \times 1$ one as well. For the hidden layer, size of W_1 is $t_1 \times n$.

The procedure of determination of the weight and bias matrix is named training. In training's iteration process, weight and bias matrices are updated according to previous matrices and a set of desired outputs for specified inputs. Although there are various training algorithms for training neurons network in literatures, the Levenberg-Marquardt

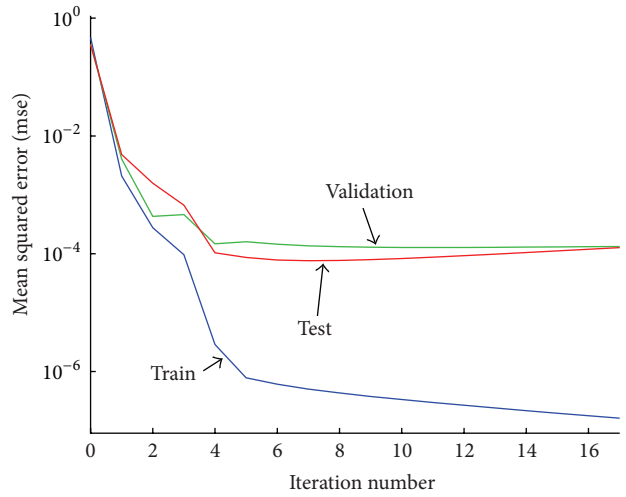

Figure 5: Performance of ANN.

Table 4: Maximum and average of errors of ANN results for all angles.

Switching angles/rad	θ_1	θ_2	θ_3	θ_4	θ_5
Maximum error/$1E-3$	3.4	8.9	5.6	1.2	0.9
Average error/$1E-4$	5.2	5.1	4.8	7.4	9.6

optimization (LMO) is chosen as it is almost the fastest back propagation algorithm. The update formulations of weight and bias matrices in LMO are

$$H = J(x)^T J(x),$$
$$g = J(x)^T e(x), \tag{11}$$
$$x_{k+1} = x_k - \left[H + \mu I\right]^{-1} g,$$

where x is the weight and bias variables matrix, $e(x)$ is the error between the desired outputs and the actual outputs of current network, $J(x)$ is the Jacobin matrix that contains the first derivatives of $e(x)$ with respect to x, and I is the identity matrix. The adaptive parameter μ is increased by a specified value in $[0, 1]$ until the performance function (mean-squared error) reaches an acceptable value.

The original data set is divided into three subsets: training, validation, and testing. The first subset is for the network training and the network is adjusted to its error. The second subject is used to measure network generalization and to halt training when generalization stops improving. The third subset provides an independent measure of network performance during and after training. The proportion of the data sample adopted in this work is 70% for training, 15% for validation, and 15% for testing.

4.2. Implementation of ANN. In order to train ANN, a set of input samples and desired outputs samples are required. In harmonic minimization problem, the inputs are modulation index and the outputs are optimal switching angles obtained by the above HPSO-TVAC. As the modulation index m^* value is a continuous variable in [0.4, 1.2], a limited number of m^* in this range are sampled. In this paper, only 40 samples are selected in [0.4, 1.2] at 0.02 interval. An ANN with 10 sigmoid neurons in hidden layer and 1 linear neuron in output layer is established to simulate the interpolation fitting problem.

As Figure 5 illustrates, the mean-squared error (MSE) is below 10^{-6} for training, 10^{-4} for validation, and 10^{-4} for testing with 17 iterations. The regression R value which measures the correlation between outputs and targets for training, validation, and testing is 0.99997, 0.99996, and 0.9995, respectively.

Table 4 shows the maximum error and the average error between the results generated by ANN and the results calculated by HPSO-TVAC for all angles in different modulation index m^*. In any modulation index value in [0.4, 1.2], compared with the results using HPSO-TVAC, the maximum and average error for all switching angles using the proposed ANN method are below 10^{-3} and are acceptable. It means that the well-designed ANN trained by 40 samples can produce almost the same optimal switching angles as the HPSO-TVAC method in the whole modulation index range. On one hand, when any DC source value varies, HPSO-TVAC algorithm must be implemented again and new switching angles must be calculated and stored in look-up tables. Look-up tables will increase dramatically when more than one DC source value change. However, the proposed ANN method can adaptively produce the optimal switching angles regardless of DC source values change. This feature is shown in the next section.

On the other hand, the computation time to produce optimal switching angles for a well-designed ANN is about 2 ms, while for HPSO-TVAC it is 0.8 s. Hence a well-trained ANN is a superior substitute for look-up tables in real-time control applications.

4.3. Compared with Previous Real-Time Algorithm. Liu et al. in [15] proposed the first real-time THD minimization algorithm for CHB converter with staircase modulation. The flow chart of this algorithm is shown in Figure 6. This method is based on the Newton-Raphson (N-R) iterative algorithm to minimize the voltage THD. There are two steps in this algorithm.

The first step is to determine the parameter ρ by solving the following equation:

$$\sum_{k=1}^{s} e_k \sqrt{1 - \left(\mu_k \rho\right)^2} = m, \tag{12}$$

where m is the given modulation index, s is the H-bridge number, and DC sources levels are $v_{dc1} \sim v_{dcs}$. Using the N-R iterative algorithm, this nonlinear equation can be solved. In the flow chart, m_c is a calculated modulation index during the iteration. If the difference between m_c and m is small enough ($<\delta$), the iteration will end and the resulting THD will be minimum. δ is the threshold value 10^{-5}.

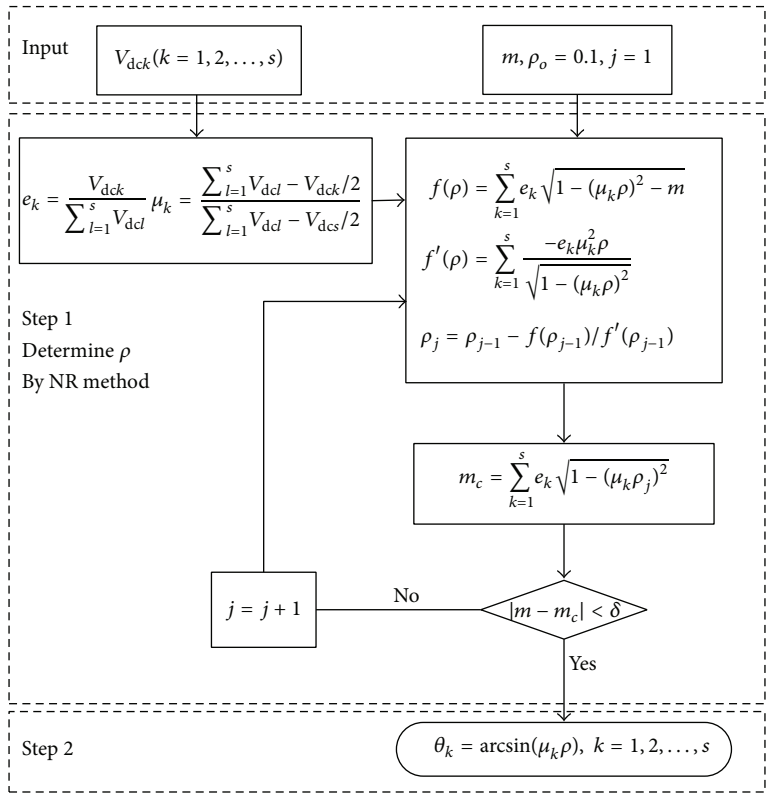

Figure 6: Flow chart of calculation in Yu's paper.

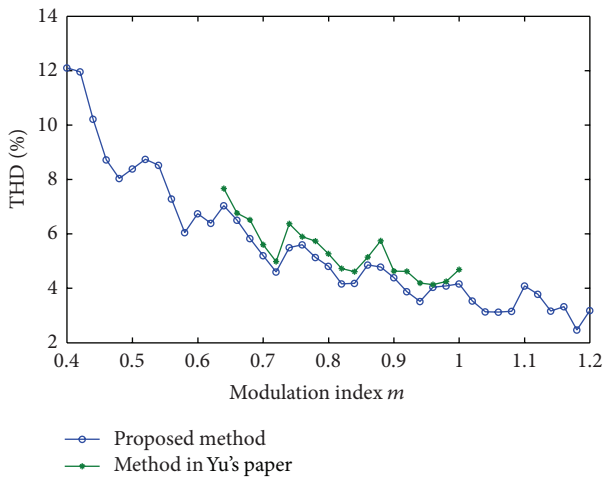

Figure 7: Comparison of THD between the proposed method and the previous method.

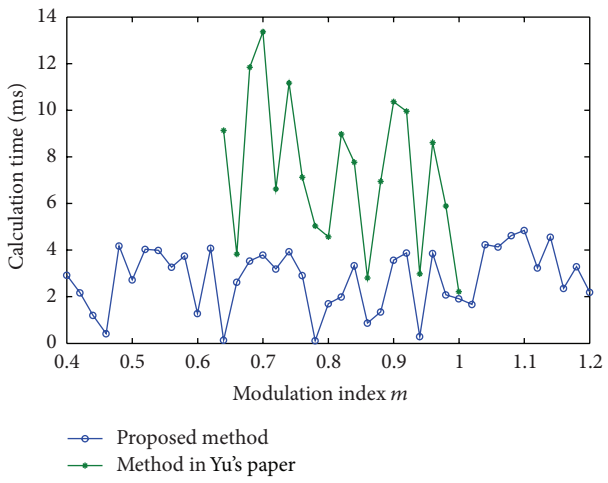

Figure 8: Comparison of calculation time between the proposed method and the previous method.

The second step is to output the optimal switching angles $\theta_1 \sim \theta_s$:

$$\theta_k = \arcsin(\mu_k \rho), \quad k = 1, 2, \ldots, s. \tag{13}$$

Taking the above five-stage 11-level CHB converter ($s = 5$) as an example, the calculated THD of the proposed method and Yu's method is compared and shown in Figure 7. The calculation time determined by the proposed method and Yu's method is also compared and shown in Figure 8.

It can be seen that the previous real-time algorithm produces almost the same optimal switching pulses and voltage THD value as the proposed method does. However, the previous method is only suitable for a small range of modulation index ([0.65–0.98]). The proposed algorithm is suitable for a wider range of modulation index ([0.4–1.2]).

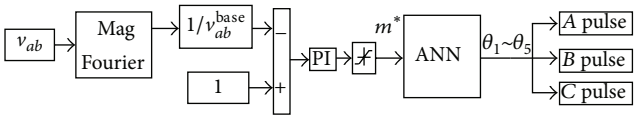

Figure 9: The proposed closed-loop control algorithm.

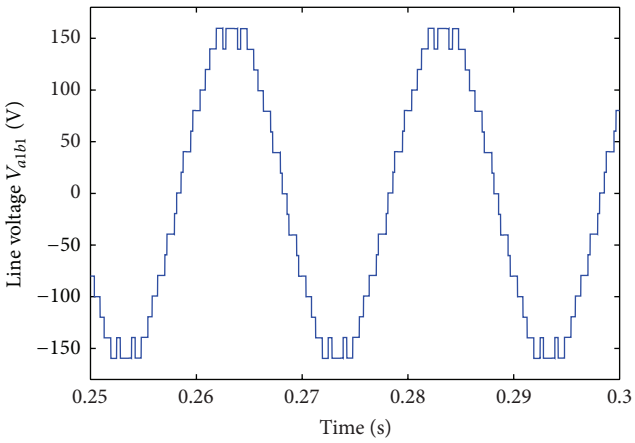

Figure 10: The converter's output line-voltage $V_{a_1b_1}$.

Table 5: Comparison of real-time algorithms.

Algorithm	Memory[17]	Cost time
N-R	25 kB	1 s
Evolution algorithm	25 kB	0.8 s
ANN	200 B	2 ms

In addition, the proposed method results in a smaller THD and a lower calculation time, compared with the previous one. The reason is that the N-R iterative algorithm is inherently sensitive to initial values. It may lose solutions in some operating points and cost more time to search for solutions in the iteration process.

Table 5 shows the cost time and memory for several methods in one running. The traditional method must store solutions for every possible operating point and the resulting memory is very large. The proposed method is adaptive and the needed memory is small. Therefore, from the point of view of the voltage THD and real-time implementation, the proposed method is better than the previous method.

5. The Proposed Closed-Loop Algorithm

The closed-loop control algorithm for three-phase CHB converter is always designed at high switching frequency (>5 k) with PSPWM or SVPWM modulation strategy. Although the classical two-loop control structure with PI controller has good dynamic performance, this high frequency method suffers high switching loss and requires many strictly equal DC sources. In this paper, a closed-loop control algorithm based on ANN for CHB converter is proposed.

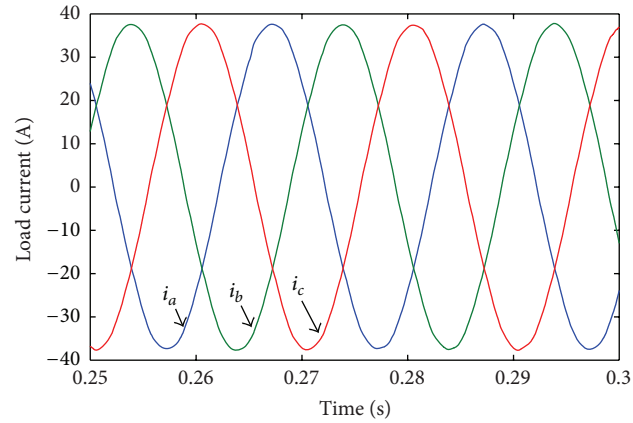

Figure 11: Three-phase load current i_{abc}.

Table 6: Parameters about 11-level CHB converter.

Power	4 kW
Filter $L_a/L_b/L_c$	4.7 mH
Load	1.875 Ω
DC voltage	20 V
Stage number	5

5.1. Closed-Loop Control Algorithm Based on ANN. As shown in Figure 1(a), the three-phase load is balanced and the load line-voltage v_{ab} is sampled to keep constant load voltage. The block diagram of proposed closed-loop control algorithm is shown in Figure 9.

A Fourier block is used to calculate the fundamental component in load line-voltage v_{ab}. The error between the desired line-voltage and the calculated one is fed to a simple PI controller. The PI controller is used to adjust the modulation index m^* and ANN is used to generate optimal switching angles $\theta_1 \sim \theta_5$ online. Pulses block is used to generate switching signals to driven H-bridges. In order to investigate the proposed closed-loop control algorithm, a test bench shown in Figure 1(a) is constructed in MATLAB/Simulink software.

Table 6 shows the 11-level CHB converter's parameters. Figure 10 shows the CHB converter's steady state output line-voltage $V_{a_1b_1}$. Figure 11 shows the three-phase load current. Harmonic analysis shows that THD of the load current is small (0.81%). The above results indicate that the proposed algorithm is effective to minimize load current's THD.

5.2. Dynamic Analysis. In real-time control applications, closed-loop control algorithm must be used to quickly stabilize load voltage and avoid current pollution when subjecting to DC sources disturbance or load disturbance. In this study, two cases are used to test the performance of the proposed closed-loop control algorithm. The proportional gain in PI controller is 1 and integral gain is 100. The sampling frequency is 10 kHz.

In Case 1, load disturbance is applied on CHB converter. The load steps form half load to full load at $t = 1.0$ s. Figure 12

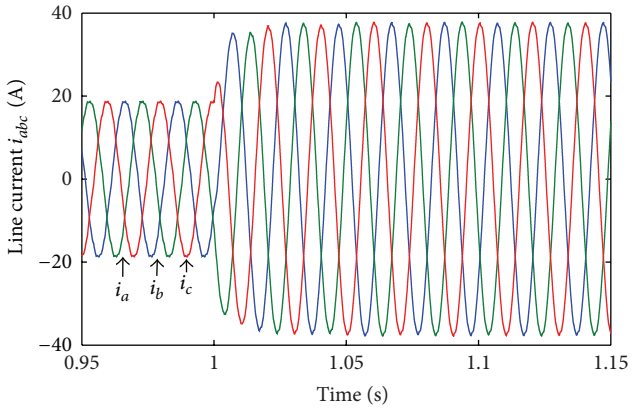

Figure 12: Three-phase load current response to load disturbance.

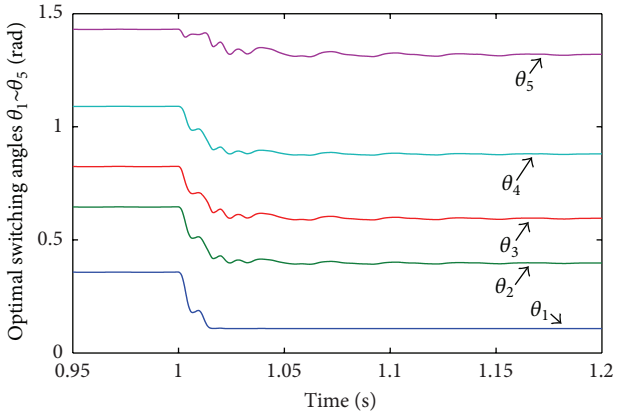

Figure 14: Optimal switching angles response to load disturbance.

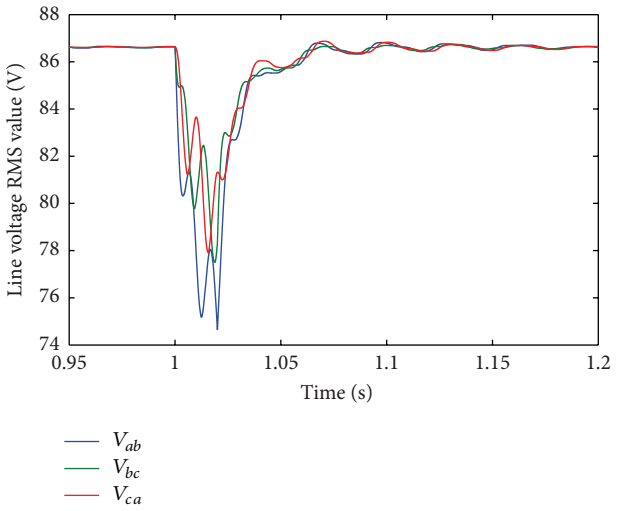

Figure 13: RMS of line-voltage response to load disturbance.

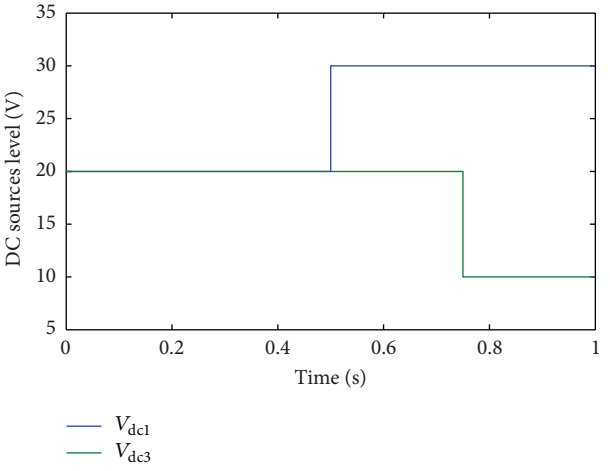

Figure 15: DC sources disturbance.

shows the corresponding line-current response. The THD of load current before and after the disturbance is 2.21% and 0.81%. Figure 13 shows the corresponding RMS of line-voltage response. Figure 14 shows the corresponding optimal switching angles response. The transient recovery time is about 0.2 s.

In Case 2, DC sources disturbance is applied on CHB converter. The first DC voltage level v_{dc1} in each phase changes from 20 V to 30 V at $t = 0.5$ s. The third DC voltage level v_{dc3} in each phase changes from 20 V to 10 V at $t = 0.75$ s. Figure 15 shows the DC voltage disturbance. Figure 16 shows the corresponding line-current response. Although the multilevel structure is considered asymmetric in this condition, the current is still balanced and has a low THD value (1.69%). Figure 17 shows the corresponding RMS of line-voltage response. Figure 18 shows corresponding optimal switching angles response.

The above results show that the proposed closed-loop control algorithm is effective to stabilize load voltage and minimize the line current's THD when subjecting to dynamic disturbance, such as DC sources disturbance and load disturbance. Especially, when the multilevel structure is considered asymmetric, the current is still balanced and avoids harmonic pollution. The CHB converter does not need many strictly equal DC sources by this algorithm, avoiding the drawbacks of traditional PSPWM or SVPWM control algorithm. The proposed closed-loop control algorithm has good control capability of CHB converter.

5.3. Real Design Issue. In real design stage, hardware implementation issue of RBF neural network and switching angles pulse generation must be considered. As the modern DSP and FPGA device's computation capability and memory increase, RBF neural network can be implemented on embedded systems. Lots of technique reports proposed various methods to address this issue [24, 25]. Thus, this section considers only the switching angles pulse generation issue.

The pulse generation can be implemented by TI DSP 28335's ePWM module. The time-based counter produces a saw-tooth waveform with a period T_w. The voltage's fundamental period is T_s. The switching angle θ is represented by an interval Δt. The corresponding switching

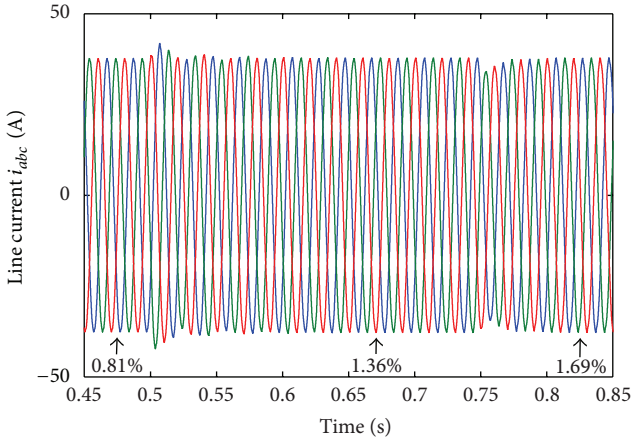

Figure 16: Three-phase load current response to DC sources disturbance.

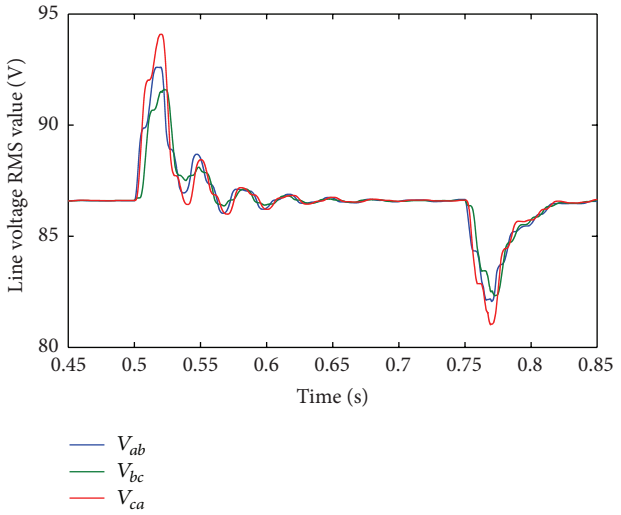

Figure 17: RMS of line-voltage response to DC sources disturbance.

signal $g_1 \sim g_4$ for four power switches S_1–S_4 in one H-bridge of CHB converter can be generated as shown in Figure 19. The H-bridge's output voltage is v_H. The high voltage level in g_i $(i = 1, 2, 3, 4)$ means that the corresponding switch S_i is turned on and low voltage level means that the corresponding switch S_i is turned off.

The turn-off time and the turn-on time for S_1 are located at i_3th and i_4th saw-tooth in interval T_s, respectively. They can be determined by ΔT_{w3} and ΔT_{w4} given as follows:

$$\Delta t = \frac{\theta}{2\pi} T_s,$$

$$i_3 = \text{Round}\left[\frac{(T_s/2 + \Delta t)}{T_w}\right],$$

$$\Delta T_{w3} = \left(\frac{T_s}{2} + \Delta t\right) - i_3 \times T_w,$$

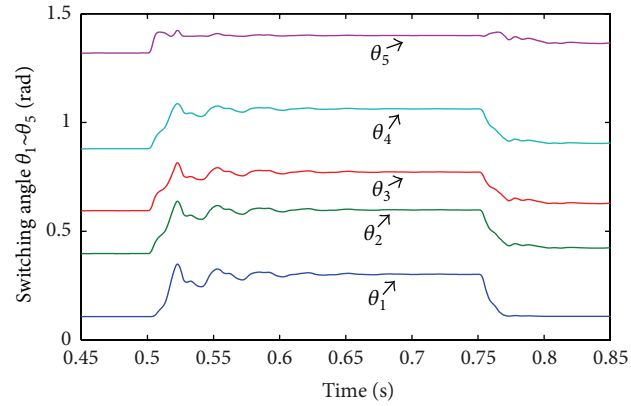

Figure 18: Optimal switching angles response to DC sources disturbance.

$$i_4 = \text{Round}\left[\frac{(T_s - \Delta t)}{T_w}\right],$$

$$\Delta T_{w4} = (T_s - \Delta t) - i_4 \times T_w. \tag{14}$$

The turn-off time and turn-on time for S_3 are located at i_1th and i_2th saw-tooth in interval T_s, respectively. They can be determined by ΔT_{w1} and ΔT_{w2} given as follows:

$$i_1 = \text{Round}\left[\frac{\Delta t}{T_w}\right], \qquad \Delta T_{w1} = \Delta t - i_1 \times T_w,$$

$$i_2 = \text{Round}\left[\frac{(T_s/2 - \Delta t)}{T_w}\right], \tag{15}$$

$$\Delta T_{w2} = \left(\frac{T_s}{2} - \Delta t\right) - i_2 \times T_w.$$

The signals, g_1 and g_2, g_3 and g_4, have opposite polarity to avoid simultaneous conduction of the upper and lower switch. As shown in Figure 19, the high level width in v_H is directly related to switching angle θ. Thus, five different width pulse voltages can synthesize the ac terminal output phase voltage v_{an} shown in Figure 1(b). When the saw-tooth waveform's period T_w is smaller, the pulse generation is more accurate.

The three-stage 7-level CHB converter's experimental output phase voltage is shown in Figure 20. The five-stage 11-level CHB converter's experimental output phase voltage is shown in Figure 21. T_s is 0.02 s for 50 Hz signal. T_w is 20 μs. Although pulses generation principle for only one operating point is given, the switching angles for other operating points can be generated similarly. The experimental results verify the proposed pulse generation scheme.

6. Conclusion

The contribution of this paper is that a real-time, closed-loop control algorithm based on ANN for three-phase CHB inverter is proposed. It costs little computation time and

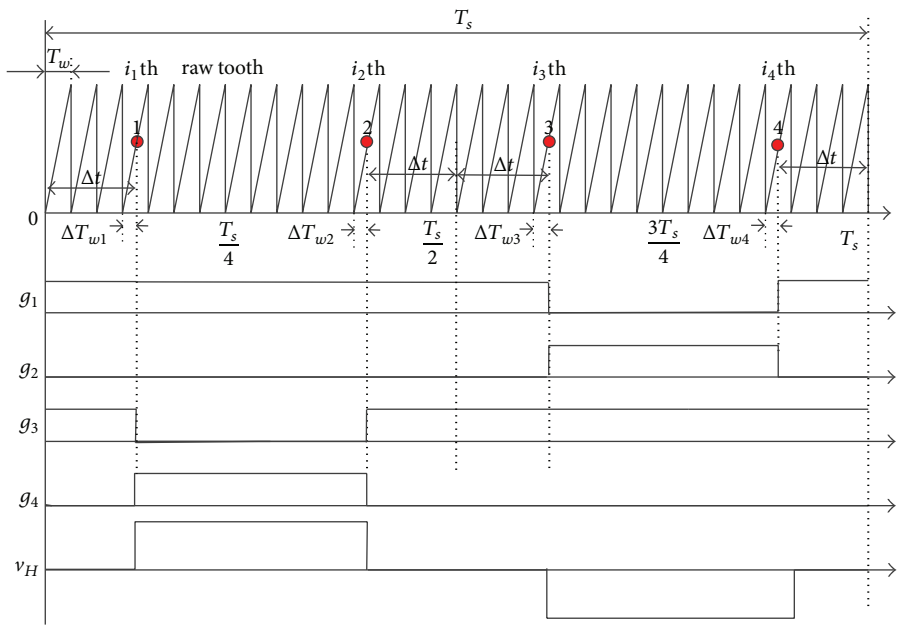

Figure 19: Proposed pulse generation scheme according to the switching angles.

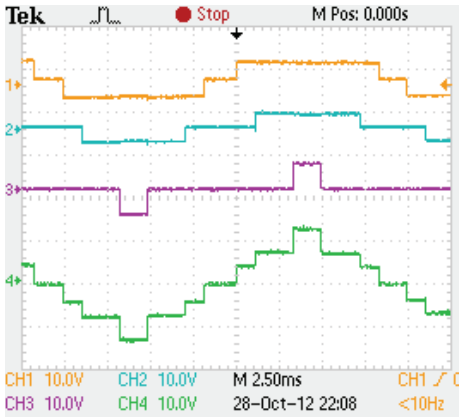

Figure 20: Three-stage 7-level staircase waveform.

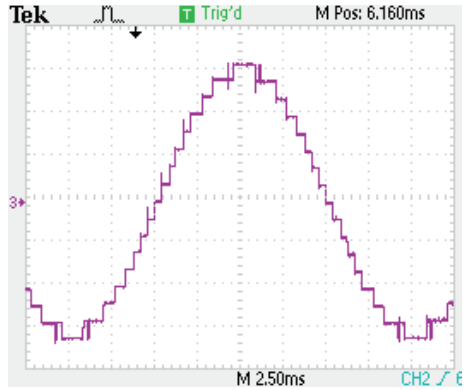

Figure 21: Five-stage 11-level staircase waveform.

memory to generate optimal switching angles and has a good control capability of CHB converter. Compared with the previous real-time optimal switching angles method, the proposed one needs little computation time and can produce better solutions in a wide modulation index [0.4–1.2]. Moreover, the proposed algorithm is closed-loop and able to quickly stabilize load voltage and minimize the line current's THD subjecting to DC sources disturbance and load disturbance. In addition, a switching angle pulse generation scheme is proposed and experiment results verify its correctness.

Conflict of Interests

The authors declare that there is no conflict of interests regarding the publication of this paper.

Acknowledgments

This work was supported by the Project of National Natural Science Foundation of China (51277083) and the Exquota Study Visit Funds China-UK (513111014).

References

[1] J. Rodríguez, J. Lai, and F. Z. Peng, "Multilevel inverters: a survey of topologies, controls, and applications," *IEEE Transactions on Industrial Electronics*, vol. 49, no. 4, pp. 724–738, 2002.

[2] M. Malinowski, K. Gopakumar, J. Rodriguez, and M. A. Perez, "A survey on cascaded multilevel inverters," *IEEE Transactions on Industrial Electronics*, vol. 57, no. 7, pp. 2197–2206, 2010.

[3] S. Sirisukprasert, J. Lai, and T. Liu, "Optimum harmonic reduction with a wide range of modulation indexes for multilevel converters," *IEEE Transactions on Industrial Electronics*, vol. 49, no. 4, pp. 875–881, 2002.

[4] P. N. Enjeti, P. D. Ziogas, and J. F. Lindsay, "Programmed PWM techniques to eliminate harmonics: a critical evaluation," *IEEE Transactions on Industry Applications*, vol. 26, no. 2, pp. 302–316, 1990.

[5] J. N. Chiasson, L. M. Tolbert, K. J. McKenzie, and Z. Du, "Elimination of harmonics in a multilevel converter using the theory of symmetric polynomials and resultants," *IEEE Transactions on Control Systems Technology*, vol. 13, no. 2, pp. 216–223, 2005.

[6] V. G. Agelidis, A. Balouktsis, and I. Balouktsis, "On applying a minimization technique to the harmonic elimination PWM control: the bipolar waveform," *IEEE Power Electronics Letters*, vol. 2, no. 2, pp. 41–44, 2004.

[7] B. Ozpineci, L. M. Tolbert, and J. N. Chiasson, "Harmonic optimization of multilevel converters using genetic algorithms," *IEEE Power Electronics Letters*, vol. 3, no. 3, pp. 92–95, 2005.

[8] M. T. Hagh, H. Taghizadeh, and K. Razi, "Harmonic minimization in multilevel inverters using modified species-based particle swarm optimization," *IEEE Transactions on Power Electronics*, vol. 24, no. 10, pp. 2259–2267, 2009.

[9] M. T. Hagh and H. Taghizadeh, "Harmonic elimination of cascade multilevel inverters with nonequal dc sources using particle swarm optimization," *IEEE Transactions on Industrial Electronics*, vol. 57, no. 11, pp. 3678–3684, 2010.

[10] B. Vasumathi and S. Moorthi, "Implementation of hybrid ANNPSO algorithm on FPGA for harmonic estimation," *Engineering Applications of Artificial Intelligence*, vol. 25, no. 3, pp. 476–483, 2012.

[11] A. Kavousi, B. Vahidi, R. Salehi, M. K. Bakhshizadeh, N. Farokhnia, and S. H. Fathi, "Application of the bee algorithm for selective harmonic elimination strategy in multilevel inverters," *IEEE Transactions on Power Electronics*, vol. 27, no. 4, pp. 1689–1696, 2012.

[12] M. S. A. Dahidah and V. G. Agelidis, "Selective harmonic elimination PWM control for cascaded multilevel voltage source converters: a generalized formula," *IEEE Transactions on Power Electronics*, vol. 23, no. 4, pp. 1620–1630, 2008.

[13] W. Fei, X. Du, and B. Wu, "A generalized half-wave symmetry SHE-PWM rormulation for multilevel voltage inverters," *IEEE Transactions on Industrial Electronics*, vol. 57, no. 9, pp. 3030–3038, 2010.

[14] M. S. A. Dahidah, G. Konstantinou, N. Flourentzou, and V. G. Agelidis, "On comparing the symmetrical and non-symmetrical selective harmonic elimination pulse-width modulation technique for two-level three-phase voltage source converters," *IET Power Electronics*, vol. 3, no. 6, pp. 829–842, 2010.

[15] Y. Liu, H. Hong, and A. Q. Huang, "Real-time calculation of switching angles minimizing THD for multilevel inverters with step modulation," *IEEE Transactions on Industrial Electronics*, vol. 56, no. 2, pp. 285–293, 2009.

[16] F. Filho, L. M. Tolbert, Y. Cao, and B. Ozpineci, "Real time selective harmonic minimization for multilevel inverters connected to solar panels using artificial neural network angle generation," in *Proceedings of the 2nd IEEE Energy Conversion Congress and Exposition (ECCE '10)*, pp. 594–598, September 2010.

[17] L. M. Tolbert, Y. Cao, and B. Ozpineci, "Real-time selective harmonic minimization for multilevel inverters connected to solar panels using artificial neural network angle generation," *IEEE Transactions on Industry Applications*, vol. 47, no. 5, pp. 2117–2124, 2011.

[18] L. G. Franquelo, J. Napoles, R. P. Guisado, J. I. León, and M. A. Aguirre, "A flexible selective harmonic mitigation technique to meet grid codes in three-level PWM converters," *IEEE Transactions on Industrial Electronics*, vol. 54, no. 6, pp. 3022–3029, 2007.

[19] A. Ratnaweera, S. K. Halgamuge, and H. C. Watson, "Self-organizing hierarchical particle swarm optimizer with time-varying acceleration coefficients," *IEEE Transactions on Evolutionary Computation*, vol. 8, no. 3, pp. 240–255, 2004.

[20] J. Kennedy and R. Eberhart, "Particle swarm optimization," in *Proceedings of the 1995 IEEE International Conference on Neural Networks*, vol. 4, pp. 1942–1948, December 1995.

[21] B. K. Bose, *Modern Power Electronics and AC Drives*, vol. 712, Prentice hall, New York, NY, USA, 2002.

[22] A. M. Trzynadlowski and S. Legowski, "Application of neural networks to the optimal control of three-phase voltag e-controlled inverters," *IEEE Transactions on Power Electronics*, vol. 9, no. 4, pp. 397–404, 1994.

[23] D. Daniolos, M. K. Darwish, and P. Mehta, "Optimised PWM inverter control using artificial neural networks," *Electronics Letters*, vol. 31, no. 20, pp. 1739–1740, 1995.

[24] S. Jung and S. S. Kim, "Hardware implementation of a real-time neural network controller with a DSP and an FPGA for nonlinear systems," *IEEE Transactions on Industrial Electronics*, vol. 54, no. 1, pp. 265–271, 2007.

[25] A. Haddoun, M. E. H. Benbouzid, D. Diallo, R. Abdessemed, J. Ghouili, and K. Srairi, "Modeling, analysis, and neural network control of an EV electrical differential," *IEEE Transactions on Industrial Electronics*, vol. 55, no. 6, pp. 2286–2294, 2008.